Equilibrium Spreading Pressure of the Mixed System of Normal Long Chain Fatty Acids

Kozo Fujii, Seiji Yoshino, Kinsi Motomura, Makoto Nakamura, and Ryohei Matuura

Department of Chemistry, Faculty of Science, Kyushu University, Fukuoka 812

(Received May 24, 1976)

Equilibrium spreading pressure were measured at various compositions and temperatures for mixed systems of tridecanoic acid-myristic acid, myristic acid-pentadecanoic acid, and pentadecanoic acid-palmitic acid, and thermodynamical treatment of these data with respect to the equilibrium between crystal and monolayer was performed. By evaluating the equilibrium composition of monolayer phase from the measured curve of equilibrium spreading pressure *vs.* composition of solid phase, the phase diagram was constructed. It was found that the equilibrium curve has a maximum point where the solid and monolayer phases have the same composition and a point where the solid phase is in equilibrium with two monolayer phases. The partial molar enthalpy change accompanied by the phase transition from solid to monolayer were found to be dependent on the composition.

It is interesting to clarify the behavior and aspect of the spreading from solid to monolayer. The equilibrium spreading pressure is related to the state of the crystal and the monolayer in equilibrium with the crystal.

Indeed the equilibrium spreading pressure (ESP) of a single component has been studied by many investigators,[1-3] but there have been much less reports about equilibrium spreading pressure of mixtures dealing with the equilibrium between the two states, namely the monolayer state and the crystal state of the mixture.[4-6]

In the present paper we intended to study the ESP of the system of tridecanoic acid-myristic acid (C_{13}–C_{14} acid system), myristic acid-pentadecanoic acid (C_{14}–C_{15} acid system), and pentadecanoic acid-palmitic acid (C_{15}–C_{16} acid system). The ESP's were measured at various compositions and temperatures, and thermodynamic treatment of the data was performed in which both the three-dimensional solid state and the two-dimensional monolayer state were taken into account on the basis of the theory in the previous paper.[7]

Experimental

Materials. The fatty acids used in the present study were purified by a fractional distillation at reduced pressure. Then they were recrystallized from petroleum ether and dried for about 24 h at room temperature under reduced pressure.

The purity was checked by differential thermal analysis (DTA), X-ray diffraction, and gas-chromatography.

Method of Measurements. A) The Measurements of Three-dimensional Solid State: Samples were prepared by melting the mixture of two acids at about 100 °C for 30 min and cooling to room temperature in a thermos bottle. Before the measurement those samples were ground in a mortor. The melting points and the transition points were measured by DTA. Long spacings of the crystal were measured by X-ray diffractometer. The details of the apparatus and method of measurements were previously described.[8]

B) The Measurements of Two-dimensional Monolayer State: Surface pressure-area measurements were performed by using a modified Wilhelmy type surface balance.

Benzene, spreading solvent, was shaken with concentrated sulfuric acid. After being washed with water to be neutral, it was refluxed with metal sodium and then carefully distilled.

The underlying solution, 0.001 M HCl, was prepared by using twice distilled water. The surface of the solution was cleaned by glass barriers coated with paraffine. The monolayer spread from benzene solution was left to stand for 10 min and then compressed continuously with a constant velocity.

C) The Measurements of ESP: Equilibrium spreading pressure measurements were performed by using an automatically recording Wilhelmy type surface balance.

Solid samples used here were the same as those described in the previous section A. After the surface of the solution was cleaned and the surface tension was held constant for more than two hours, an amount of powdered sample was deposited on it.

The pressure increased as time passed and reached a value which was held constatnt within ± 0.2 dyn/cm per hour. We took it as the ESP.

Results and Discussion

Three-dimensional Solid State. The melting points, the transition points, and the freezing points measured by DTA, and the long spacings measured by X-ray diffraction for the C_{13}–C_{14} system are plotted against the composition in Figs. 1 and 2, respectively. Similar results were also obtained for the C_{14}–C_{15} and C_{15}–C_{16} systems. From these results we assume that the solid

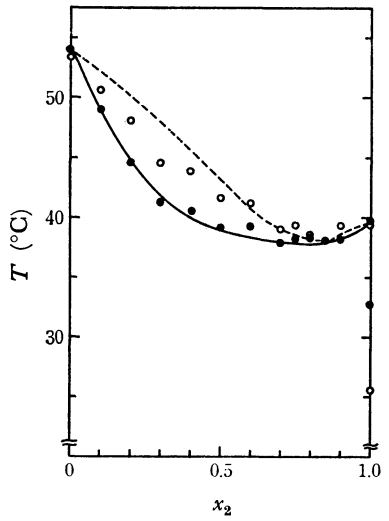

Fig. 1. Melting point, transition point, and freezing point *vs.* mole fraction of tridecanonic acid curves of the C_{13}–C_{14} system : ●, heating; ○, cooling; ——, solidus curve given by Eq. 4 ; ----, liquidus curve given by Eq. 5.

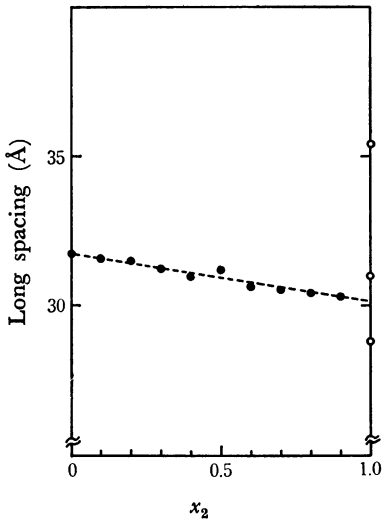

Fig. 2. Long spacing *vs.* mole fraction of tridecanoic acid curve of the C_{13}–C_{14} the system.

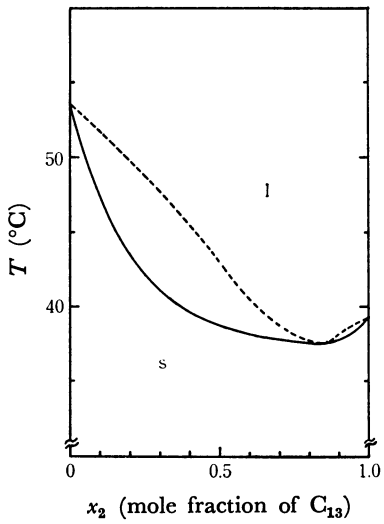

Fig. 3. Three-dimensional phase diagram of the C_{13}–C_{14} system : l, region of liquid solution; s, region of solid solution.

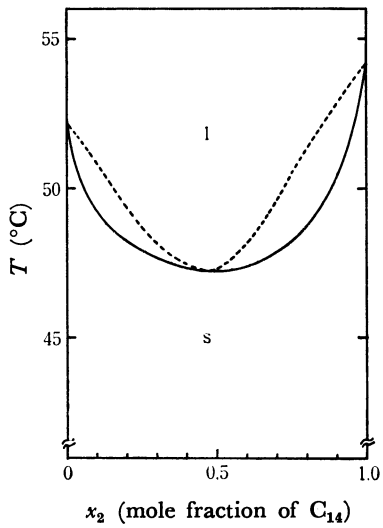

Fig. 4. Three-dimentional phase diagram of the C_{14}–C_{15} system : l, region of liquid solution; s, region of solid solution.

state is the regular solution, because the solid state deviates from ideal in such an extent that the curve representing the equilibrium between solid and liquid phases has a small minimum. And the liquid phase is assumed to be an ideal solution. Then we apply an equation similar to that for azeotropic mixture of liquid-vapor system. We have the following equations[9]

$$(\omega/RT_A)(x^s_{1,A})^2 = (\Delta h^0_1/R)(1/T_A - 1/T^0_1) \quad (1)$$

and

$$(\omega/RT_A)(x^s_{1,A})^2 = (\Delta h^0_2/R)(1/T_A - 1/T^0_2) \quad (2)$$

where Δh^0_i is the heat of fusion, T^0_i is the melting point, T_A is the temperature of minimum point, $x^s_{i,A}$, is the mole fraction of ith component at the minimum point, ω is a constant relating to the interaction energy, the superscript s denotes solid phase, and the subscripts 1 and 2 denote the fatty acids of larger and smaller carbon number, respectively. From Eqs. 1 and 2, we obtain

$$\omega = \{[\Delta h^0_1(T^0_1 - T_A)/T^0_1]^{1/2} + [\Delta h^0_2(T^0_2 - T_A)/T^0_2]^{1/2}\}^2 \quad (3)$$

The values of Δh^0_i, T^0_i, T_A, and ω for each system are listed in Table 1. Then, we can calculate the solidus and liquidus curves from the following equations;

$$x^s_2 = \{\exp[\omega(x^{s2}_2/RT) - \lambda_1] - 1\}/\{\exp[\omega(x^{s2}_2/RT) - \lambda_1] - \exp[\omega(x^{s2}_1/RT) - \lambda_2]\} \quad (4)$$

and

$$x^l_2 = \{\exp[\omega((x^{s2}_1 + x^{s2}_2)/RT) - \lambda_1 - \lambda_2] - \exp(-\lambda_2)\}/\{\exp[\omega(x^{s2}_2/RT) - \lambda_1] - \exp[\omega(x^{s2}_1/RT) - \lambda_2]\} \quad (5)$$

where

$$\lambda_1 = (\Delta h^0_1/R)(1/T - 1/T^0_1) \quad (6)$$

and

$$\lambda_2 = (\Delta h^0_2/R)(1/T^0_2 - 1/T). \quad (7)$$

So, we can depict the phase diagram, which is shown in Figs. 3 to 5 for the C_{13}–C_{14}, C_{14}–C_{15}, and C_{15}–C_{16} systems, respectively. These systems show minimum points, but there are small differences between the values of mole fraction of minimum point. It is concluded that in binary solid mixtures the different behavior is arisen from the difference in the crystalline state between an odd-numbered acid and an even-numbered acid.

Two-dimensional Monolayer State. It is impossible to perform thermodynamic analysis with respect to the ESP if we do not have information of the state of monolayer. So the surface pressure-mean molecular area (π-A) curve was measured at various compositions and temperatures. It was found that in each system the transition pressure from expanded to condensed state, π^{eq}, varied somewhat linearly with the mole fraction of component 2 referred to the fatty acids, x^π_2, over the whole range of composition.

The composition of the condensed film (c) coexisting with the expanded film (e) is calculated by using the equation [7,11]

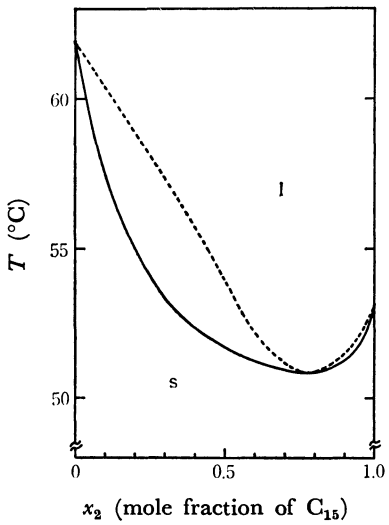

Fig. 5. Three-dimensional phase diagram of the C_{15}–C_{16} system : l, region of liquid solution; s, region of solid solution.

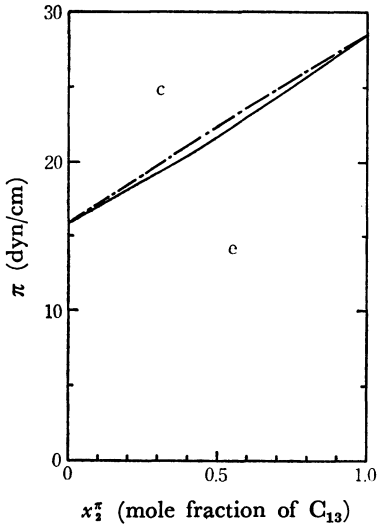

Fig. 6. Two-dimensional phase diagram of the C_{13}–C_{14} system at 20 °C : c, region of condensed monolayer; e, region of expanded monolayer.

$$x_2^{\pi,c} = x_2^{\pi,e} + [(A^c - A^e)x_1^{\pi,e}x_2^{\pi,e}/kT](\partial\pi^{eq}/\partial x_2^{\pi,e})_{p,T} \quad (8)$$

By a procedure similar to that in the previous paper,[11,12] the phase diagrams of two-dimensional monolayer state were depicted for each system in Figs. 6 to 8. The aspect of these phase diagrams is quite identical. After all, it is concluded that the two-component fatty acid system in which the number of carbon atoms is different by only one gives almost ideal mixture in monolayer state.

Equilibrium between Solid State and Monolayer State.

When a sample of fatty acid mixture is placed on the surface of water, the surface pressure increases with time as it spreads on the surface. The surface pressure-time curve is shown in Fig. 9 for the C_{14}–C_{15} system as an example.

The break point is detected at $x_2^s = 0.75$ and 0.10, but not at 0.90. The surface pressure at the break

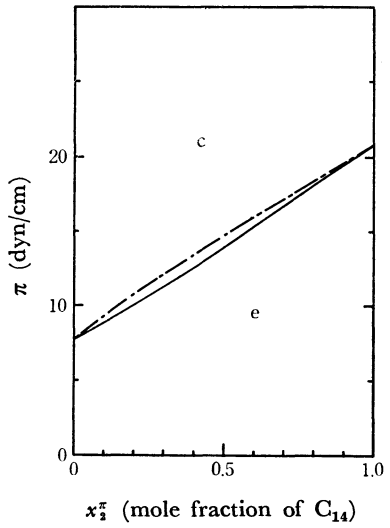

Fig. 7. Two-dimensional phase diagram of the C_{14}–C_{15} system at 25 °C : c, region of condensed monolayer; e, region of expanded monolayer.

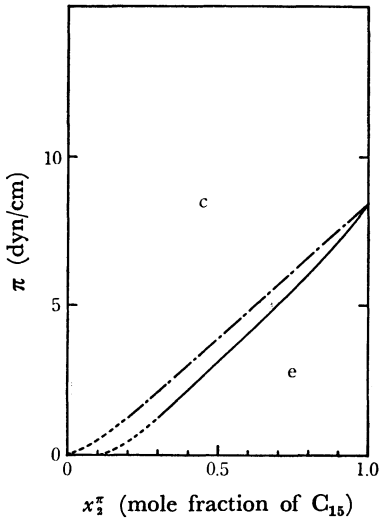

Fig. 8. Two-dimensional phase diagram of the C_{15}–C_{16} system at 25 °C : c, region of condensed monolayer; e, region of expanded monolayer.

point is almost equal to that of transition from the expanded to the condensed film. So it is expected that the phase transition occurs at the break point and therefore the monolayer in equilibrium with the bulk solid forms a condensed film. Consequently it is concluded that the break point is observed if bulk solid is in equilibrium with the condensed film, but not observed if bulk solid is in equilibrium with the expanded film.

The values of ESP measured at various compositions and temperatures are plotted against the compositions of the bulk solid for the C_{14}–C_{15} system in Fig. 10. The similar curves were also obtained for other two systems. Comparing the ESP curves with the solidus curve in Fig. 4, it seems likely that the higher the melting points, the lower the ESP, and *vice versa*. We may say that the solid sample having the higher melting point is more difficult to spread because of its stronger molecular

Table 1. The calculated values of ω for each system

Fatty acid	Heat of fusion[10] (kcal/mol)	Mixture	Minimum point (°C)	ω (cal/mol)
Tridecanoic acid (C_{13})	8.02			
		C_{13}-C_{14} system	311.1	835.0
Myristic acid (C_{14})	10.74			
		C_{14}-C_{15} system	320.2	756.9
Pentadecanoic acid (C_{15})	10.30			
		C_{15}-C_{16} system	323.9	708.5
Palmitic acid (C_{16})	12.98			

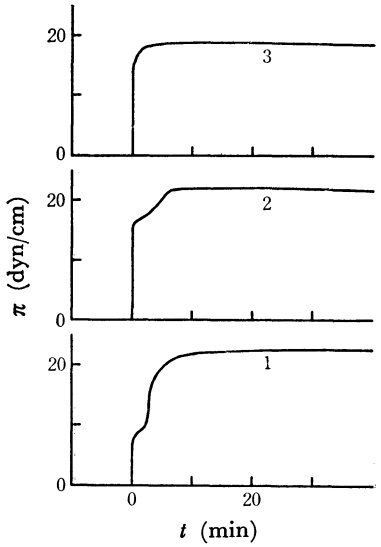

Fig. 9. Spreading pressure *vs.* time curve of the C_{14}–C_{15} system at 25 °C : 1, x_2^s=0.10; 2, 0.75; 3, 0.90.

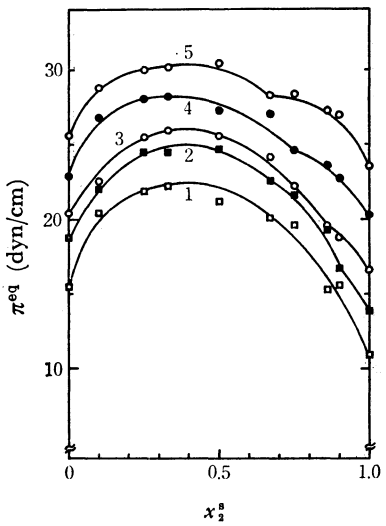

Fig. 10. Equilibrium spreading pressure *vs.* mole fraction of myristic acid curves of C_{14}–C_{15} system : 1, 15 °C; 2, 20 °C; 3, 25 °C; 4, 30 °C; 5, 35 °C.

interaction.

In Fig. 10 the break points are observed on ESP curves at 20, 25, 30, and 35 °C. For the C_{13}–C_{14} acid system the break points were observed at 25 and 30 °C, while for the C_{15}–C_{16} system the break point was not observed in the range of experimented temperatures. It might be presumed that at this break point two monolayer phases are formed by spreading from the crystal. This is understood from the fact that the curve 3 in Fig. 10 and the curves in Fig. 7 intersect in the neighborhood of that break point.

We shall consider thermodynamically the behavior of the variation of ESP with the composition shown in Fig. 10. Choosing the mole fraction x_2^s as a free variable, the variation of the ESP, π^{eq}, with x_2^s can be written in the following form[7,11]

$$(\partial\pi^{eq}/\partial x_2^s)_{T,p} = [(\partial\mu_1^s/\partial x_2^s)(\partial\mu_2^m/\partial x_2^\pi) - (\partial\mu_2^s/\partial x_2^s)(\partial\mu_1^m/\partial x_2^\pi)] / [\bar{a}_1^\pi(\partial\mu_2^m/\partial x_2^\pi) - \bar{a}_2^\pi(\partial\mu_1^m/\partial x_2^\pi)] \quad (9)$$

In Eq. 9, $\bar{a}_i^\pi$ is the apparent partial molar area related to the mean molar area, a, as

$$\bar{a}_1^\pi = a - x_2^\pi(\partial a/\partial x_2^\pi) \quad (10)$$

$$\bar{a}_2^\pi = a + x_1^\pi(\partial a/\partial x_2^\pi) \quad (11)$$

From the Gibbs-Duhem equation in the bulk phase, we have

$$x_1^s(\partial\mu_1^s/\partial x_2^s) + x_2^s(\partial\mu_2^s/\partial x_2^s) = 0 \quad (12)$$

and in the monolayer phase, we have

$$x_1^\pi(\partial\mu_1^m/\partial x_2^\pi) + x_2^\pi(\partial\mu_2^m/\partial x_2^\pi) = 0 \quad (13)$$

Substituting Eqs. 10 to 13 into Eq. 9;

$$(\partial\pi^{eq}/\partial x_2^s)_{T,p} = [(x_2^\pi - x_2^s)/x_1^s a](\partial\mu_2^s/\partial x_2^s)_{T,p} \quad (14)$$

If $(\partial\mu_2^s/\partial x_2^s)_{T,p}$ is known, the mole fraction of the equilibrium monolayer coexisting with crystal, x_2^π, can be calculated. In the previous section we have assumed the solid solution as the regular solution; *i.e.*,

$$RT\ln\gamma_1^s = \omega(x_2^s)^2 \quad (15)$$

and

$$RT\ln\gamma_2^s = \omega(x_1^s)^2 \quad (16)$$

where γ_i^s is the activity coefficient in bulk solid. The chemical potential in the bulk solid is expressed in terms of the composition as

$$\mu_2^s = \mu_2^{0,s} + RT\ln x_2^s + \omega(x_1^s)^2 \quad (17)$$

Differentiating the above equation with respect to x_2^s at constant T and p and substituting it into Eq. 14, we obtain the equation for calculating x_2^π:

$$x_2^\pi = x_2^s + [ax_1^s x_2^s/(RT - 2\omega x_1^s x_2^s)](\partial\pi^{eq}/\partial x_2^s)_{T,p} \quad (18)$$

Since it has been established that the mixed monolayers of long chain n-fatty acids have the same molar area, irrespective of the chain length, if they are in the same monolayer state, [11–13] the values of a were determined from the π-A curve of C_{14} acid when the equilibrium monolayer is the expanded film and that of C_{18} acid when the equilibrium monolayer is the condensed film.

It is now possible to make up the phase diagram of

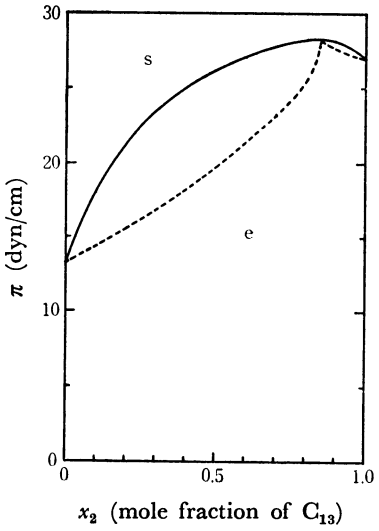

Fig. 11. Phase diagram of the C_{13}–C_{14} system at 20 °C : s, region of solid solution; e, region of expanded monolayer.

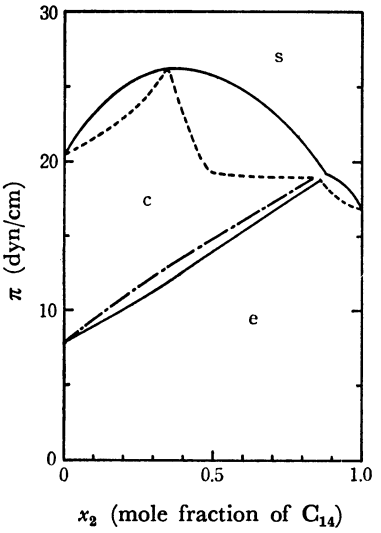

Fig. 12. Phase diagram of the C_{14}–C_{15} system at 25 °C : s, region of solid solution; c, region of condensed monolayer; e, region of expanded monolayer.

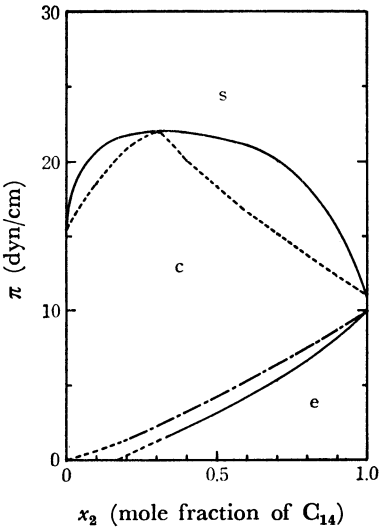

Fig. 13. Phase diagram of the C_{14}–C_{15} system at 15 °C: s, region of solid solution; c, region of condensed monolayer; e, region of expanded monolayer.

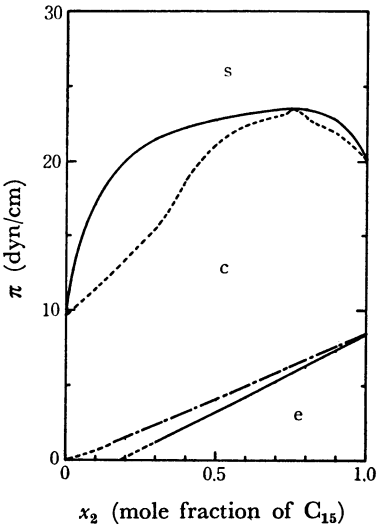

Fig. 14. Phase diagram of the C_{15}–C_{16} system at 25 °C: s, region of solid solution; c, region of condensed monolayer; e, region of expanded monolayer.

the mixed system of fatty acids representing the condition of equilibrium between phases of solid and monolayer, which is illustrated in Figs. 11 to 14 for the present three systems at different temperatures. In Fig. 11 of the C_{13}–C_{14} system it is shown that the bulk solid is in equilibrium with the expanded film at any composition, but in Fig. 14 of the C_{15}–C_{16} system the bulk solid is in equilibrium with the condensed film. In the case of the C_{14}–C_{15} system, the phase diagram at 15 °C drawn in Fig. 13 is similar to that of the C_{15}–C_{16} system. However, the phase diagram at 25 °C drawn in Fig. 12 is different from the above ones in that the bulk solid is in equilibrium with the condensed film in the portion of mole fraction from $x_2^\pi=0$ to 0.85, but in the portion of mole fraction from $x_2^\pi=0.85$ to 1.0 the bulk solid is in equilibrium with the expanded film. At this point, that is, at the mole fraction of $x_2^\pi=0.85$, the bulk solid, the condensed film, and the expanded film coexist. This is the triple point. As seen in Fig. 10, this point shifts to a higher value of x_2^s with decreasing temperature. This triple point disappears at 15 °C in the C_{14}–C_{15} system. Though there is a possibility of appearance of the triple point in the C_{15}–C_{16} system if the temperature is raised, we can not experiment at the higher temperature because of several restrictions.

Entropy and Enthalpy Changes Accompanied by the Phase Transition from Bulk Solid to Equilibrium Monolayer.

Now, from the variation of the transition pressure with temperature, the entropy changes accompanied by the phase transition from solid state to monolayer state can be calculated by using equation [7,11]

$$(\partial\pi^{eq}/\partial T)_{p,x_2^s} = [(\bar{s}_1^\pi-\bar{s}_1^s)(\partial\mu_2^m/\partial x_2^\pi) - (\bar{s}_2^\pi-\bar{s}_2^s)(\partial\mu_1^m/\partial x_2^\pi)] / [\bar{a}_1^\pi(\partial\mu_2^m/\partial x_2^\pi)-\bar{a}_2^\pi(\partial\mu_1^m/\partial x_2^\pi)] \quad (19)$$

Substituting Eqs. 10, 11, and 13 into Eq. 19, we obtain the following equation

$$a(\partial\pi^{eq}/\partial T)_{p,x_2^s} = x_1^\pi(\bar{s}_1^\pi - \bar{s}_1^s) + x_2^\pi(\bar{s}_2^\pi - \bar{s}_2^s) \quad (20)$$

The calculation of the apparent mean molar entropy change of the C_{14}–C_{15} system was carried out at 20 °C by making use of the values of $(\partial\pi^{eq}/\partial T)_{p,x_2^s}$ estimated from Fig. 10. The entropy changes plotted against the composition of the equilibrium monolayer, x_2^π, are shown in Fig. 15. It exhibits a remarkable discontinuity at the mole fraction of $x_2^\pi \approx 0.9$, and separates into two parts. It seems to be the reason for the discontinuity that the entropy of spreading to expanded film differs considerably from that to condensed film. The magnitude of this gap is fairly good agreement with the value taken at the corresponding mole fraction from Fig. 16 where the apparent mean molar entropy change, $[x_1^{\pi,c}(\bar{s}_1^{\pi,c} - \bar{s}_1^{\pi,e}) + x_2^{\pi,c}(\bar{s}_2^{\pi,c} - \bar{s}_2^{\pi,e})]$, associated with the transition from expanded to condensed monolayer is plotted against the mole fraction of the expanded monolayer, $x_2^{\pi,e}$. For the C_{15}–C_{16} system the entropy change calculated similarly indicated that the phase transition occurs from solid state to condensed film over the whole range of the composition.

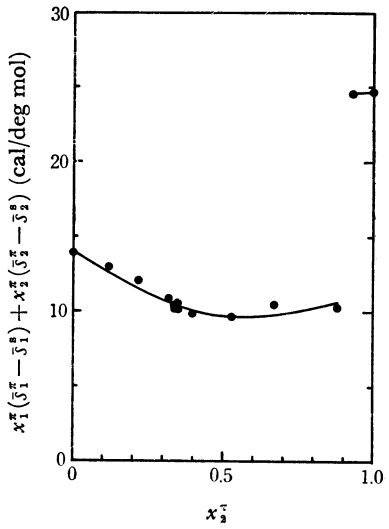

Fig. 15. Apparent mean molar entropy change *vs.* mole fraction of myristic acid curve of the C_{14}–C_{15} system at 20 °C.

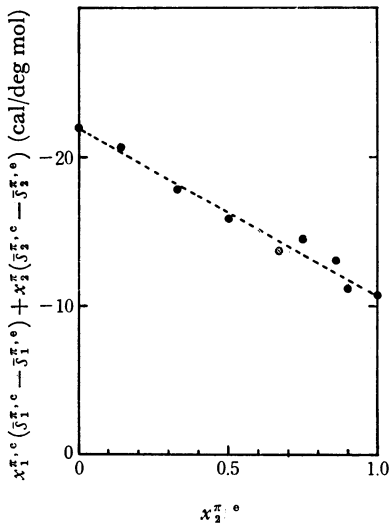

Fig. 16. Apparent mean molar entropy change *vs.* mole fraction of myristic acid curve of the C_{14}–C_{15} system at 20 °C.

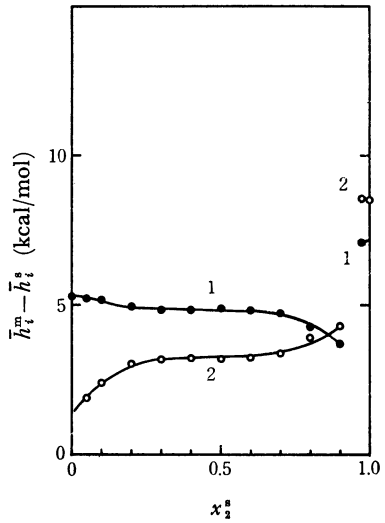

Fig. 17. Partial molar enthalpy change *vs.* mole fraction of myristic acid curve of the C_{14}–C_{15} system at 20 °C : 1, pentadecanoic acid; 2, myristic acid.

Each term of the right-hand side of Eq. 20 is the apparent partial molar entropy change of the respective component and is connected with the partial molar entropy change at the phase transition from the solid to the monolayer state, $\bar{s}_i^m - \bar{s}_i^s$, by

$$\bar{s}_1^m - \bar{s}_1^s = (\bar{s}_1^\pi - \bar{s}_1^s) - [a - x_2^\pi(\partial a/\partial x_2^\pi) - \bar{a}_1](\partial\pi/\partial T)_{p,x_w^m,x_2^\pi} - \bar{a}_1(\partial\gamma^0/\partial T)_p \quad (21)$$

and

$$\bar{s}_2^m - \bar{s}_2^s = (\bar{s}_2^\pi - \bar{s}_2^s) - [a + x_2^\pi(\partial a/\partial x_2^\pi) - \bar{a}_2](\partial\pi/\partial T)_{p,x_w^m,x_2^\pi} - \bar{a}_2(\partial\gamma^0/\partial T)_p \quad (22)$$

where $\bar{s}_i$ is partial molar entropy, $\bar{a}_i$ is the partial molar area, x_w^m is the mole fraction of water in the monolayer and γ^0 is the surface tension of pure water.[7,11] Further we can calculate the partial molar enthalpy change by

$$\bar{h}_1^m - \bar{h}_1^s = T(\bar{s}_1^m - \bar{s}_1^s) \quad (23)$$

and

$$\bar{h}_2^m - \bar{h}_2^s = T(\bar{s}_2^m - \bar{s}_2^s), \quad (24)$$

where $\mu_i^m = \mu_i^s$ has been used.

The results are shown in Fig. 17 for the C_{14}–C_{15} system at 20 °C where we have plotted it against the composition of solid state. From this figure the partial molar enthalpy change may be said to be dependent on the composition. On the other hand, the partial molar enthalpy change from expanded to condensed film, $\bar{h}_i^e - \bar{h}_i^c$, is almost independent of the composition.[12] This difference in the composition dependence of the partial molar enthalpy change seems to result from the non-ideal behavior in solid solution or from the fact that the ESP changes with the size of solid grain which is spread.[14]

References

1) W. D. Harkins and G. C. Nutting, *J. Am. Chem. Soc.*, **61**, 1702 (1939).
2) W. D. Harkins, T. F. Young, and G. E. Boyd, *J. Chem. Phys.*, **8**, 954 (1940).
3) G. E. Boyd, *J. Phys. Chem.*, **62**, 536 (1958).
4) M. Nakagaki and N. Funasaki, *Bull. Chem. Soc. Jpn.*, **47**, 2094 (1974).
5) M. Nakagaki and N. Funasaki, *Bull. Chem. Soc. Jpn.*, **47**, 2482 (1974).
6) P. Joos, *J. Colloid Interface Sci.*, **35**, 215 (1971).
7) K. Motomura, *J. Colloid Interface Sci.*, **48**, 307 (1974).
8) Y. Moroi, T. Hiraharu, S. Yoshino, and R. Matuura, *Mem. Fac. Sci. Kyushu Univ.*, **C8**, 43 (1972).
9) I. Prigogine and R. Defay, "Chemical Thermodynamics," Longmans, Green & Co. Ltd., London (1954), p. 450.
10) W. E. Garner and A. M. King, *J. Chem. Soc.*, **1926**, 2491; *ibid*, **1929** 1894.
11) K. Motomura, K, Sekita, and R. Matuura, *J. Colloid Interface Sci.*, **48**, 319 (1974).
12) K. Sekita, M. Nakamura, K. Motomura, and R. Matuura, *Mem. Fac. Sci. Kyushu Univ.*, **C10**, 51 (1976).
13) N. Kuramoto, K. Sekita, K. Motomura, M. Nakamura, and R. Matuura, *Mem. Fac. Sci. Kyushu Univ.*, **C8**, 67 (1972).
14) K. Motomura, *J. Colloid Interface Sci.*, **23**, 313 (1967).